ELSEVIER

Earth and Planetary Science Letters 150 (1997) 7–26

EPSL

# Erosion and rift dynamics: new thermomechanical aspects of post-rift evolution of extensional basins

E. Burov [a,1,2], S. Cloetingh [b,*]

[a] *BRGM, Orléans, France*

[b] *Faculty of Earth Sciences, Vrije Universiteit, Amsterdam, The Netherlands*

Received 9 October 1996; revised 1 April 1997; accepted 2 April 1997

**Abstract**

In this study, we investigate thermo-mechanical consequences of erosion of rift shoulders. Conventional models imply post-rift cooling that results in subsidence and strengthening of the lithosphere. Existing models neglect geodynamic consequences of surface processes (erosion and sedimentation). According to sedimentologic and geomorphologic data, surface processes modify the topography and thickness of sedimentary infill at rates comparable with the rates of the tectonic uplift/subsidence (few 0.1 mm/y). Consequently, a coupling between the surface and tectonic processes can be expected. An increase of the sedimentary load leads to localised inelastic weakening of the lithosphere. At the same time, erosional unloading of rift shoulders leads to local strengthening and flexural rebound. Subsidence of the rift "neck" (strongest layer of the thinned lithosphere) and uplift of the rift shoulders create pressure gradients sufficient to drive ductile flow in the low-viscosity lower crust. This flow, directed outward from the centre of the basin might facilitate uplift of the rift shoulders. It may even drive some post-rift "extension". In the limiting case of slow erosion and sedimentation rates, gravitational stresses can reverse the flow, resulting in a retardation of basin subsidence rate, homogenisation of the crustal thickness, accelerated collapse of the shoulders and in some post-rift "compression". These effects significantly change predictions of basin evolution inferred from the conventional back-stripping models. © 1997 Elsevier Science B.V.

*Keywords:* extension tectonics; erosion; sedimentation; rift zones; rheology

## 1. Introduction

As it is most commonly accepted (i.e., [1–3]) subsidence of extensional basins results from transient conductive cooling of initially thinned and heated lithosphere (Fig. 1). Most of the proposed mechanisms relate thinning to pure-shear extension caused by various processes such as necking or mantle extension [4,5]. Most of the existing models (except, may be, [6]) separate mechanisms of crustal thinning from the processes of sedimentation and erosion of the elevated flanks, though some studies considered effects of thermal insulation due to accumulation of low-conductivity matter [7]. More general investigations of thermal effects of surface processes on continental geotherms [8,9] have shown that these processes can significantly retard cooling,

* Corresponding author.

[1] On leave from CGDS/Institute of Physics of the Earth, Moscow, Russia.

[2] Previously at Institut de Physique du Globe de Paris, France.

0012-821X/97/$17.00 © 1997 Elsevier Science B.V. All rights reserved.
*PII* S0012-821X(97)00069-1

change $P$–$T$ paths, and stratigraphic patterns. However, a possible interdependence between the sedimentation, subsidence and rheological behaviour of the lithosphere has not been really studied.

Escarpments at rifted margins are believed to be caused by one or a number of processes: lateral heat transport, dynamic effects (spatial variations of the extension rate), flexural forces, small-scale convection or underplating [10–13]. In all cases, the evolution of the rift basin and shoulders should be essentially controlled by re-distribution of surface loads due to surface processes. Observed erosion rates are typically highest along the slopes and edges of the escarpments (hillslope erosion), and the lowest in the hinterland [14]. This leads to preferential removal of the material in zones of elevated and recent (i.e., rough) topography, and its accumulation in the central parts of the rifted basins. Such additional vertical loads exerted on the lithosphere (several km of sediments) can create bending stresses of hundreds of MPa. According to rock mechanics data, these stresses should lead to weakening of the lithosphere (see [15] for a review, also [13,16]) which would result in more "localized" mass compensation in the central parts of the basin and in maintenance of a higher strength closer to the margins [17]. Such effects are actually observed (e.g., [18]). The load-dependent non-linear properties of the lithosphere should also affect the subsidence phases, traced via the records of vertical motions inferred from tectonic geomorphology and fission-track age/length patterns [19].

Uplift of the flanks must be linked with the subsidence of the basin. The flanks undergo erosion which controls re-filling of the rift basin with sediments. The sedimentary deposits typically exceed 5–10 km in depth (e.g., Pannonian basin, Albert rift, Baikal rift). The associated vertical load is much greater than that associated with the rift flanks (typically 1–2 km high, Fig. 2).

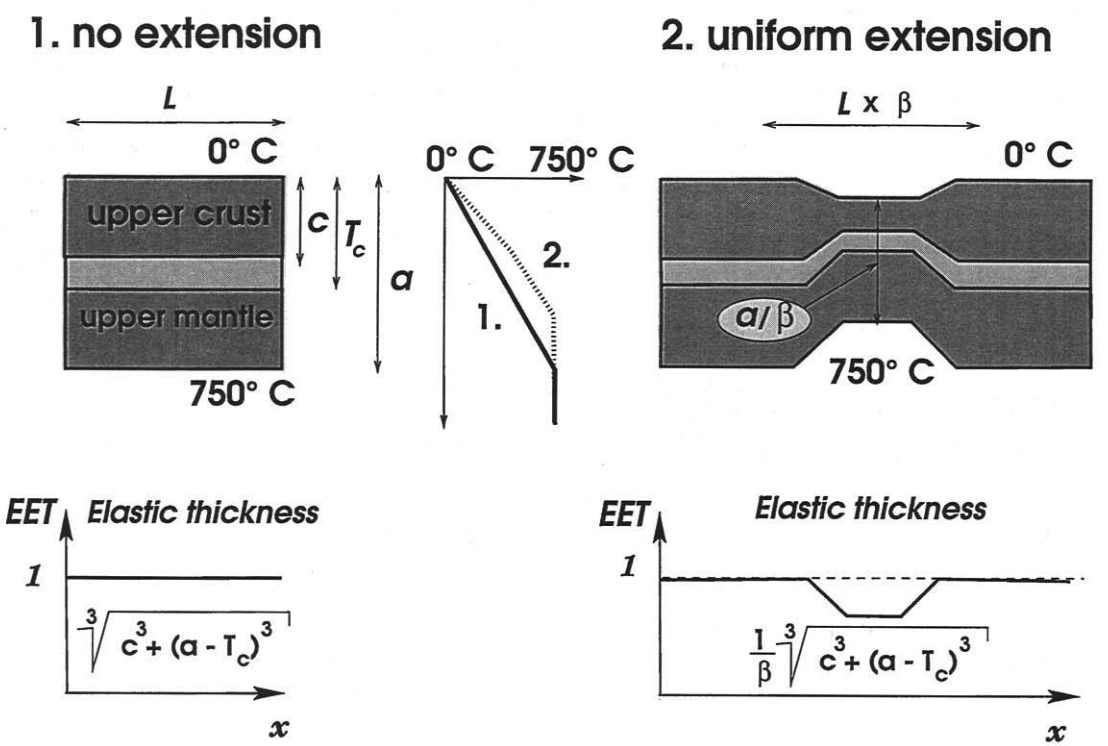


Fig. 1. Cartoon showing adopted classical McKenzie [1] model of thermal subsidence. *Top*: Initially homogeneous lithosphere (*left*, length of a sample segment $L$, thickness $a$, thickness of upper crust $c$, total thickness of crust $T_c$) is instantly extended by pure shear (*right*). Length of segment will be $L \times \beta$ whereas thickness of extended lithosphere will be $a/\beta$. *Middle*: corresponding behaviour of effective elastic thickness (EET).

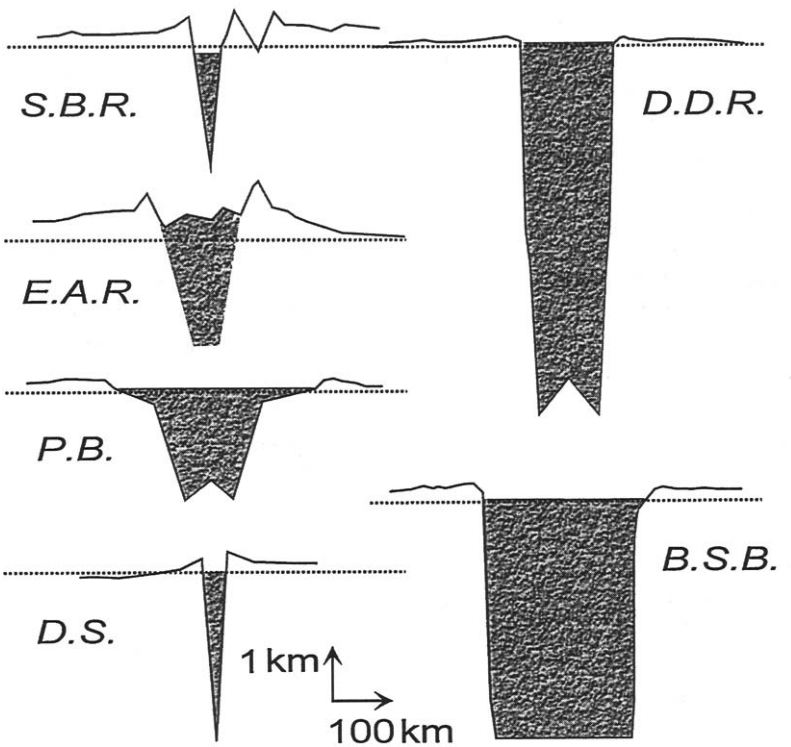


Fig. 2. Sketch cross-sections of several flexural rifts systems with important amount of sedimentary deposits: South Baikal rift (*S.B.R.*) [53,54]; East African rift (*E.A.R.*) [13,48,41]; Dnieper–Donets rift (*D.D.R.*) [55]; Pannonian basin (*P.B.*)[56]; Black Sea basin (*B.S.B.*) [57]; Dead Sea (*D.S.*) [58].

For a quartz-dominated rheology, the viscosity of the lower crust can be 2–3 orders lower than that of the upper crust (e.g., [20]). In this case, pressure gradients maintained by erosion- and temperature-controlled subsidence of the basin and by the flank uplift, may drive shear flow in the weak lower crust (e.g., [21–26]). In its turn, this flow may further facilitate the flank uplift and subsidence of the basin. The crustal flow may exert some horizontal shear traction on the strong/weak crustal interface and thus lead to additional extension. When the erosion is slow, subsidence of the basin might be retarded due to gravity-driven pressure gradients associated with density contrasts between the crust and mantle lithosphere. Such pressure gradients can drive horizontal spreading of the thicker crustal roots beneath the elevated topography (rift flanks). If the flexural strength of the lithosphere is not sufficient to support rift shoulders, they will collapse.

In the present study, we demonstrate the importance of sedimentation and erosion for the mechanisms of crustal thinning and shoulder uplift. We test our ideas through examination of surface evolution and mechanical response of competent and ductile horizons of the lithosphere beneath post-rift basins. Consideration of the non-linear reaction of the competent lithosphere constitutes an important difference with most conventional models which assume a linear response to the time-dependent loading (or unloading) of the lithosphere (e.g., [3,14]).

## 2. Model for thermomechanical evolution of post-rift basin coupled with surface processes: basic components

At least three vertical mechanical loads act on the lithosphere: (1) positive surface loads (topography

and deposited eroded material); (2) negative loads due to erosion in the uplifted areas; and (3) restoring (e.g., isostatic) response of the lithosphere that tends to compensate changes in (1) and (2), as well as changes due to cooling or flow in the lower crust. The response of the lithosphere depends on its rheological properties and thermal state. Thus the general model components are: (a) a surface processes model; (b) a rheological model of the lithosphere; and (c) a model of the thermomechanical response to surface and subsurface loads. The evolution of surface loads due to sedimentation/erosion is described by phenomenologically determined laws of erosion and surface transport [27,28,12]. The rheology laws are known from experimental rock mechanics (e.g., [29,20]). They can be constrained using additional multidisciplinary data (e.g., [17,16,30,10,31,32]). The model of the mechanical response of the lithosphere requires solution of the equations of mass, momentum and energy conservation.

Below we describe in detail the different components of the model.

## 2.1. Surface processes

Erosion ($\Delta E$) and denudation represent the integrated effect of processes of removal of overburden rocks. The residual surface uplift ($U$) has two components, $h_t$ and $w$ [33]. $h_t$ is referred to as the contribution by tectonic forces (compression, thermal expansion, etc.), whereas $w$ presents the isostatic response. The relation between uplift and erosion is given by:

$$w + h_t = \Delta E + h_0 - h_i$$

where $\Delta E$ is the thickness of the eroded section; $h_0$ is the present elevation; and $h_i$ is the initial paleo-elevation. Later in this paper we denote the observed rate of the surface topographic elevation/subsidence as $\mathrm{d}h(x,t)$, the cumulative rate of the tectonic uplift and isostatic response as $\mathrm{d}u(x,t)$, and the rate of the erosion/denudation as $\mathrm{d}e(x,t)$:

$$\partial u(x,t)/\partial t = \partial h(x,t)/\partial t + \partial e(x,t)/\partial t$$

The tectonic-scale transport equations describe long-term changes in topography $h(x,y,t)$ as a result of simultaneous short- and long-range mass transport processes [12,34].

### 2.1.1. Short-range surface processes

The short-range surface processes are represented by cumulative effects of hillslope processes (soil creep, rainsplash, slides) that remove material from uplifted areas and transport it to the valleys [27,35]. The sum of these processes can be represented as linear downslope diffusion of material volume: the horizontal material flux, $q_s$ is related to local slope, $\nabla h$, by $q_s = -K_s \nabla h$, where $K_s$ is the effective diffusivity, e.g. $K_s = U_s h_s$, and $U_s$ is the transport speed of an erodible surface layer of thickness $h_s$ [12]. Different values of $K_s$ correspond to different lithologies. Assumption of conservation of mass volume leads to the linear diffusion equation for erosion:

$$\partial h/\partial t = K_s \nabla^2 h \qquad (1)$$

Eq. (1) can be solved with constant-elevation boundary conditions simulating local base levels of erosion. Short-range hillslope erosion leads to smoothing of topography. The diffusive sediment flux ($q_s$) tends to zero at a drainage divide/flank, but the change of sediment flux $\mathrm{d}q_s/\mathrm{d}x$ remains finite [36]. A drainage divide or flank axis migrates from one side to the other toward the lower curvature side at a rate proportional to the change in curvature ($\mathrm{d}^3h/\mathrm{d}x^3$) [34].

The erodibility might depend on slope and curvature of topography. This can be described by more realistic non-linear diffusion equations of the form:

$$\partial h/\partial t = k^*(x,h,\nabla h)\nabla^2 h \qquad (2)$$

in which $k^*(x,h,\nabla h)$ would be height, distance, slope or curvature dependent. Hereafter we will only consider a non linear expression of the form $k^*(x,h,\nabla h) = k(x)(\nabla h)^n$ [28]. The empirical Eq. (2) differs from that obtained assuming a non-linear diffusion coefficient in Eq. (1). We will refer to the cases with $n = 1, 2$ as to the first- and second-order short-range diffusion, respectively.

### 2.1.2. Long-range transport processes

The long-range transport processes represent the cumulative effect of fluvial transport of the suspended load and bedload:

$$q_{fe} = -K_r q_r \mathrm{d}h/\mathrm{d}l \qquad (3)$$

where $q_r$ is river discharge; $dh/dl$ is the slope in the direction of the river drainage; $K_f$ is a non-dimensional transport coefficient; and $l$ is the distance along the transporting channel. Several studies employ a non-linear discharge dependence for sediment transport (e.g., [37,38]), as suggested by theoretical

Table 1
Definition of variables and parameters

| Variable/parameter | Values and units | Definition | Comments |
|---|---|---|---|
| $\tau_{xx}$, $\tau_{xy}$, $\tau_{yy}$, $\sigma_{xx}$, $\sigma_{xy}$, $\sigma_{yy}$ | Pa, MPa | stress components | $\sigma\tau - PI$ |
| $P$ | Pa, MPa | pressure | |
| $v$ | m/s, mm/y | velocity vector | or tensor |
| $u$, $v$ | m/s, mm/y | velocity components | $xx$ and $yy$, respectively |
| $\mu$ | Pa s | effective viscosity | $10^{19}$–$10^{23}$ Pa s |
| $k$ | $m^2/y$ | coefficient of erosion | ≈ mass diffusivity |
| $dh$ | m, km | topographic uplift | or subsidence |
| $du$ | m, km | tectonic uplift | do not mix with $u$ |
| $de$ | m, km | erosion | or sedimentation |
| $\dot{\varepsilon}$ | $s^{-1}$ | average strain rate | $\dot{\varepsilon} = (\frac{1}{2}\dot{\varepsilon}_{ij}\dot{\varepsilon}_{ij})^{1/2}$ |
| $E$ | $8 \times 10^{10}$ N/m$^2$ | Young's modulus | |
| $\nu$ | 0.25 | Poisson's ratio | |
| $A^*$ | $Pa^{-n}$ $s^{-1}$ | material constant | power law (Tables 1 and 2) |
| $n$ | 3–5 | stress exponent | power law (Table 2) |
| $H^*$ | kJ $mol^{-1}$ | activation enthalpy | power law (Table 2) |
| $R$ | 8.314 J/mol K | gas constant | power law (Table 2) |
| $T$ | °C, K | temperature | |
| $w$, $w(x)$ | m, km | vertical plate deflection | mantle lithosphere mostly |
| $T_e$, $\tilde{T}_e(x,w,w',w'',t)$ | m, km | effective elastic thickness EET | |
| $h(x,t)$ | m, km | surface topography | |
| $\tilde{h}(x,t)$ | m, km | upper boundary of ductile channel | |
| $h_c$, $T_c$ | m, km | Moho depth | Moho boundary |
| $h_{c2}$ | m, km | lower boundary of ductile crust | $h_{c2} \le T_c$ |
| $h_{c1}(x,t,w)$ | m, km | upper-crustal mechanical thickness | here, 10–20 km |
| $\Delta h_{c2}(x,t,w,u,v)$ | m, km | thickness of crustal channel | $\Delta h_{c2} = h_{c2} - h_{c1}$ |
| $h_2(x,t,w,u,v)$ | m, km | thickness of the mechanical mantle | $h_2 = a - T_c$ |
| $a(x,t,w,u,v)$ | m, km | mechanical bottom of the mantle | ≈ depth to 750°C |
| $\rho_s$ | 2300 kg/m$^3$ | density | of sediments |
| $\rho_{c1}$ | 2650 kg/m$^3$ | density | of upper crust |
| $\rho_{c2}$ | 2900 kg/m$^3$ | density | of lower crust |
| $\rho_m$ | 3330 kg/m$^3$ | density | of mantle |
| $\beta$, $\gamma$ | | coefficients of rift extension | crust and mantle, respectively |
| $g$ | 9.8 m/s$^2$ | acceleration due to gravity | |
| $t_a$ | m.y. | thermal age | ≤ geological age |
| $a_t$ | 250 km | thermal thickness of the lithosphere | depth to 1330°C |
| $T_m$ | 1330°C | $T$ at depth $a$ | |
| $\chi_{c1}$ | $8.3 \times 10^{-7}$ m$^2$ $s^{-1}$ | thermal diffusivity | upper crust |
| $\chi_{c2}$ | $6.7 \times 10^{-7}$ m$^2$ $s^{-1}$ | thermal diffusivity | lower crust |
| $\chi_m$ | $8.75 \times 10^{-7}$ m$^2$ $s^{-1}$ | thermal diffusivity | mantle |
| $k_{c1}$ | 2.5 W $m^{-1}$ $K^{-1}$ | thermal conductivity | upper crust |
| $k_{c2}$ | 2 W $m^{-1}$ $K^{-1}$ | thermal conductivity | lower crust |
| $k_m$ | 3.5 W $m^{-1}$ $K^{-1}$ | thermal conductivity | mantle |
| $h_r$ | 10 km | decay scale for radiogenic heat | upper crust |
| $H_s$ | $9.5 \times 10^{-10}$ W $kg^{-1}$ | radiogenic heat production rate | upper crust |
| $H_{c2}C_{c2}^{-1}$ | $1.7 \times 10^{-13}$ K $s^{-1}$ | radiogenic heat | lower crust |
| $\rho_{c1}C_{c1p}$ | $3 \times 10^6$ J $(m^3$ $K)^{-1}$ | density × specific heat | upper crust |
| $\rho_{c2}C_{c2p}$ | $3 \times 10^6$ J $(m^3$ $K)^{-1}$ | density × specific heat | lower crust |
| $\rho_m C_{pm}$ | $4 \times 10^6$ J $(m^3$ $K)^{-1}$ | density × specific heat | mantle |

(e.g., [38]) and empirical studies of sediment transport on short time scales [27].

*2.1.3. Numerical implementation of the surface models*

The tectonic and isostatic components of uplift are resolved by backstacking the inferred amount of eroded material onto the present-day topography (e.g., [14]) and by integrating the model differential equations on a discrete topography [34]. The model time step $\Delta t$ is limited by the stability condition and was equal to 20 years in our calculations. The landscape evolution is calculated by updating the topography at the end of each time step for the effects of denudation, isostatic readjustment and tectonic deformation.

## 2.2. Rheology

We adopt brittle–elasto-ductile rheologies based on the rock mechanics data for quartz-dominated crust and olivine-dominated mantle, considered as the most representative composition for the continental lithosphere [20,29]. This model implies power law stress and exponential temperature dependence of the strain rates ($\dot{\varepsilon}$) within the ductile parts of the lithosphere [20,29]: $\dot{\varepsilon} = A^* \exp(-H^*/RT)(\sigma_1 - \sigma_3)^n$, where $T$ is the absolute temperature at the given depth (Appendix A); $\sigma_1$ and $\sigma_2$ are the principal stresses; and $A^*$, $H^*$, $R$, and $n$ are the material constants explained in Table 2. The brittle strength (Byerlee's law, [15]) is linearly proportional to pressure, and is higher for compression (depth gradient $\approx 0.66 \times 10^5$ Pa/m) than for tension (depth gradient $\approx 0.22 \times 10^5$ Pa/m). The elastic, or quasi-elastic behaviour is given by linear stress/strain relation assuming typical Young's modulus and Poisson's ratio (Table 1, [39]).

*2.2.1. Yield–stress envelope*

Combined, the constitutive laws form vertical rheological profiles (yield–stress envelopes) used for the modelling of the mechanical response of the lithosphere (Table 2). Dependent on the geotherm, mineral composition and content of fluids (Table 2), the effective viscosity drops from $10^{22}$–$10^{23}$ Pa s in the upper crust/upper mantle to an "asthenospheric" value of $10^{19}$–$10^{20}$ Pa s in the lower crust. Rock mechanics literature proposes quite different rheological parameters for quartz-controlled rheologies. However, recent discussions [20] point out that the choice of "weakest" rheological parameters is more reasonable. Such generally neglected factors as thermal blanketing of the upper crust and shear heat dissipation in the lower crust can increase the temperature by 50–100°C, which may be large enough to bring the crustal strength down to the lowest estimates.

*2.2.2. Deep seismicity and ductile lower crust*

Deep seismic events (> 20 or even > 40 km) observed in some rift systems (e.g., Baikal [40], East Africa, Rhine graben [41]) are sometimes interpreted in terms of a strong lower-crustal rheology. However, variation of unstable-to-stable frictional slip on the deeply penetrating faults and local accelerations of the strain rate can essentially increase ductile strength in a narrow band allowing for deep brittle-

Table 2
Parameters of dislocation creep for major lithospheric rocks and minerals [60–62,29,15]

| Mineral/rock | $A^*$ ($Pa^{-n}$ $s^{-1}$) | $H^*$ (kJ $mol^{-1}$) | $n$ |
|---|---|---|---|
| Quartz (dry) | $2.710^{-20}$ | 156 | 2.4 |
| Quartz (dry) | $6.03 \times 10^{-24(a)}$ | 134 | 2.72 |
| Quartz (wet) | $1.3 \times 10^{-20}$ | 134 | 2.4 |
| Quartz (wet) | $1.26 \times 10^{-13(a)}$ | 172.6 | 1.9 |
| Olivine/dunite (dry) dislocation climb at $\sigma_1 - \sigma_3 \leq 200$ MPa | $7 \times 10^{-14}$ | 520 | 3 |
| Olivine (Dorn's dislocation glide) at $\sigma_1 - \sigma_3 \geq 200$ MPa) | $\dot{\varepsilon} = \dot{\varepsilon}_0 \exp[-HU\{1-(\sigma_1-\sigma_3)/\sigma_0\}^2/RT]$ where $\dot{\varepsilon}_0 = 5.7 \times 10^{11}$ $s^{-1}$, $\sigma_0 = 8.5 \times 10^3$ MPa; $H^* = 535$ kJ $mol^{-1}$ | | |

Quartz rheologies marked with ([a]) are used in the given study.

to-ductile transitions. Presence of a strong lower crust requires higher EET values than are actually observed [17].

### 2.3. Thermomechanical response of the lithosphere to surface and subsurface loads

#### 2.3.1. Mechanical and geometrical considerations

The general question which we address is to test if the dynamic pressure differences created by erosion/sedimentation in the lower crust could compensate any other non-hydrostatic pressure components (hardly above 50 MPa, maximum 100 MPa). The dynamic pressure component is proportional to $2\mu * \dot{\varepsilon}$. For the ductile flow this value equals the yielding strength. Such flow stress requires viscosities in the range of $10^{19}$–$10^{21}$ Pa s at strain rates $10^{-13}$–$10^{-15}$ $s^{-1}$. These values fall in the range of the typical continental parameters (e.g., assuming subsidence rate $\approx \partial e/\partial t = 1$ mm/y on a horizontal scale of 100 km, we get $\dot{\varepsilon}_{yy} \approx \mathrm{d}(\partial e/\partial t)/\mathrm{d}x \approx 3 \times 10^{-11}$ m $s^{-1} * 10^{-5}$ $m^{-1} \approx 10^{-15}$ $s^{-1}$).

The evolution of the "sub-surface" lithosphere in the most general form is governed by mass, momentum and energy conservation equations:

$$\begin{cases} \partial\rho/\partial t + \mathrm{div}(\partial \boldsymbol{v}) = 0 \\ \mathrm{div}\,\sigma + \rho g = 0 \\ \rho C_p \cdot \partial T/\partial t - \mathrm{div}(\boldsymbol{k}\nabla T) + \boldsymbol{v}\nabla T = H_r + H_d \end{cases} \quad (4)$$

where $\rho$ is the density; $\boldsymbol{v}$ is velocity tensor; $g$ is the acceleration due to gravity; $\sigma$ is the stress tensor; $C_p$ is the specific heat; $\boldsymbol{k}$ is the thermal conductivity tensor; and $H_r$ and $H_d$ are the radiogenic and dissipative heat production per unit volume, respectively (see [42] and Table 1). England and Richardson [8] have shown that the thermal effect $\partial T/\partial t$ of the tectonic uplift caused by erosion is proportional to $u_x \cdot \partial T/\partial x$, where $u_x = \partial h/\partial t$ represents the upward movement of the material cased by flexural rebound in response to surface unloading.

In most practical cases, Eqs. (4) can be solved only using a purely numerical scheme (e.g., [13,16]). Specifically, we adopted the finite-element code "tecton" originally developed by Melosh and Raefsky (e.g., [43]).

To have some control on the physics of the modelled processes, and save computing time, we also adopted a semi-analytical model based on several commonly used approximations. The flow in the lower-crustal channel is approximated using a channel flow formulation (see Appendix A, Table 1 and more details in [22,24,42]). The channel flow approximation describes the evolution of a thin subhorizontal layer of a viscous or ductile power law medium underlaid by a Winkler-type basement [44,22,24]. The walls of the channel are formed by the strong parts of the upper crust and upper mantle and may become thinner or thicker due to inelastic yielding and horizontal deformation. The mechanical response of the walls is modelled using the plate approximation with brittle–elasto-ductile rheology (Appendix B, [17]).

In the model, the inelastic upper wall of the ductile channel is loaded with the surface topography. The model topography is modified by the erosion, flexure and flow in the ductile channel. In general, our semi-analytical model is close to that proposed by Avouac and Burov [42] for compressive orogenic belts.

### 2.4. Coupled integrated model

The equations for the channel stresses, laminar flow velocities and thickness of the ductile layer (Appendix A) are linked together with the heat transfer equations (Appendix A) and, via stress and velocity continuity conditions, with the equations of flexure of the competent portions of the upper crust and mantle lithosphere (Appendix B, [17]). The equations of erosion (1)–(3) are solved on each time step to compute normal load (topography) changes. This constitutes the complete system of equations describing the evolution of the system in time.

This formulation allows us to model both the rift and post-rift stages, but we restrict our modelling to investigation of the post-rift stage only. We consider the following general scenario (Fig. 3). The initial temperature distribution and geometry correspond to that produced by McKenzie's model [1] with several modifications, explained below in the text. Using this temperature distribution, geometry and predefined initial topography, we first solve the plate flexure problem and the initial flow problem in the lower crust (moment of time $t = 0$). This state corre-

sponds to the time when the rapid (instantaneous in McKenzie's model) stage of rifting stops. At this time, the erosion is switched on and the basin begins to be filled with sediments derived from erosion on its slopes. On each numerical time step, the topography is updated and flexure and flow are recalculated again. The temperature structure of the lithosphere evolves according to the 2-D heat transfer model (Appendix A). The accumulation of the sediments results in an increase of the load exerted on the rift basin. The lithosphere flexes and becomes weaker due to the flexural stresses. This weakening helps localise tectonic movements and results in a migration of the rift neck.

The described semi-analytical approach is based on several approximations which are not required in a pure numeric model (finite-element in our case) based on solution of Eqs. (4). However, in the case of large strength variations, most straightforward numerical approaches are computationally intensive, and their results require additional interpretations. Thus analytical-numerical cross-checks are very use-

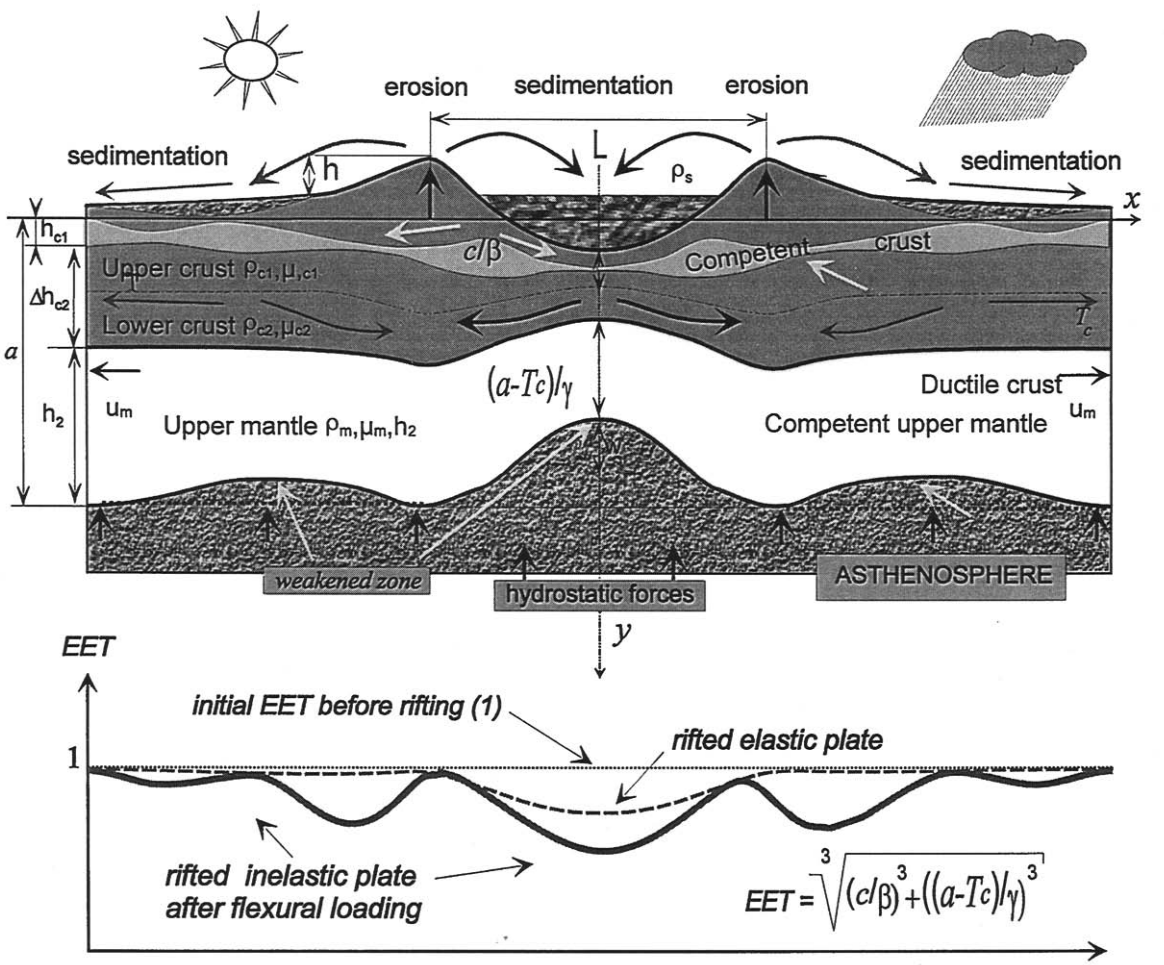


Fig. 3. Proposed scenario of basin subsidence: sediments (density $\rho_s$) derived from erosion on slopes of rift shoulders result in increase of load on basin. Strong parts of the crust (density $\rho_{c1}$, non-Newtonian viscosity $\mu_{c1}$, thickness $h_{c1}$) and of mantle lithosphere ($\rho_m$, $\mu_m$, $h_m$) flex and weaken (weak zones are marked by *white arrows*). As a result, EET drops beneath the basin and shoulders (*bottom*) and becomes lower than the EET immediately after extension. Lower-crustal material ($\rho_{c2}$, $\mu_{c2}$, $h_{c2}$) flows from centre of basin towards the shoulders, facilitating their uplift. Spreading velocity $u_m$ can be additionally assigned at the base of the crust. Following [2], different coefficients of extension can be assumed for the crust and mantle lithosphere ($\beta$ and $\gamma$, respectively). Other conventions are as in Fig. 1 and Table 1.

ful. We later show that the results of purely numerical experiments were highly consistent with our asymptotic results, therefore justifying the selected approach.

*2.4.1. Boundary and initial conditions*

We have chosen simplest boundary conditions corresponding to the plate and flow approximations (Appendices A and B). The velocity boundary conditions are assumed on the bottom interface of the lower-crustal channel, the horizontal shear stress and the vertical stress are zero at the surface of the Earth. The normal stress at the base of the crust is defined by the condition of the regional isostatic compensation, and is computed from the solution of the inelastic plate flexure problem (Appendix B). Free flow is the inherent lateral boundary condition. The velocity boundary conditions can also be combined with a

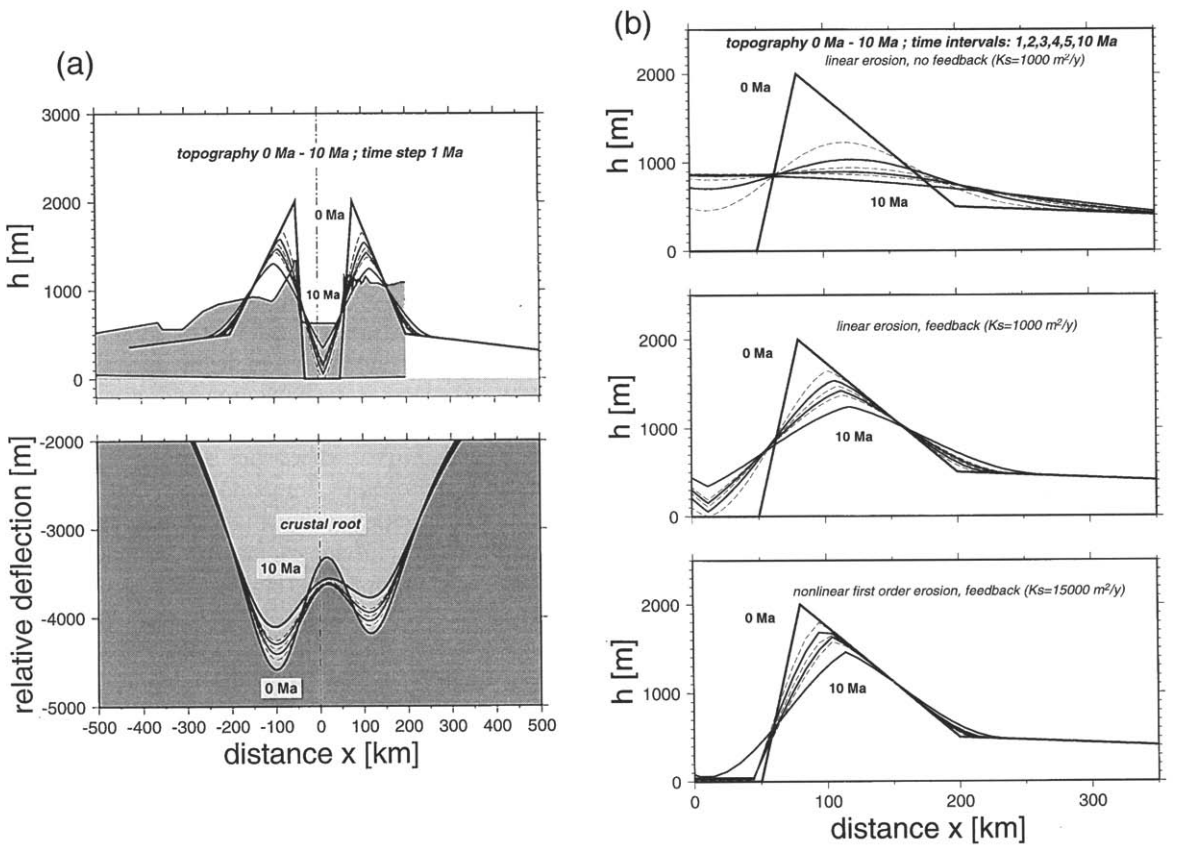


Fig. 4. a. Evolution of a synthetic landform (*top*) and deflection of the underlying Moho (*bottom*) due to coupled surface processes (linear erosion with $k = 1000$ m$^2$/y) and flow in lower crust. *Lines* correspond to 1, 2, 3, 4, 5 and 10 Ma. For comparison, present-day topographic segment of Albert rift (East Africa) is shown (background). Erosion/sedimentation rates vary in time reaching $> 0.2$ mm/y on the rift shoulders. However, due to compensatory mechanisms, resulting surface rate does not exceed 0.1 mm/y. Coefficient of extension $\beta = 1.5$.

b. *Top*: Evolution of a synthetic rift flank in assumption of no feedback between erosion and subsurface processes. Strong linear erosion ($k = 1000$ m$^2$/y) rapidly wipes out the escarpment. *Middle*: Same as top but with coupling between surface and subsurface processes. Rift flank persists. *Bottom*: Same as middle but with non-linear erosion law ($k = 15000$ m$^2$/y). Rift flank is well preserved in time. Note erosional retreat of the escarpment. For old rifts ($> 50$ Ma) this retreat may be hundreds of km.

pre-defined lateral pressure gradient. The competent and ductile parts of the lithosphere interact through the conditions of continuity of stress and velocity.

The choice of boundary conditions is not a simple problem. Some authors apply vertically homogeneous stress, force or velocity on the sides of the model plate, Winkler-type forces as bottom vertical condition, and free surface/normal stress as an upper boundary condition [13,45]. Other authors use shear traction (velocity/stress) on the bottom of the mantle lithosphere [46,26,47]. Constant-force boundary conditions may lead to significantly different results [45]. All what we know about boundary conditions in nature comes from geodetic and geophysical measurements of the surface strain rates and velocities. These data are insufficient to distinguish between different models because the relation between the surface deformations with those at depth is unclear. We thus have chosen the simplest conditions.

The initial conditions (temperature and initial subsidence rate) naturally correspond to those inferred from the "reference" McKenzie [1] model. McKenzie's coefficient of extension, $\beta$, used in our calculations, varied between 1.25 and 3 (as in many rift systems [48,31,30,32]). However, we "correct" McKenzie's model in two points: (1) a 2-D thermal conduction equation is solved instead of a 1-D one (Eqs. 4, Appendix A); and (2) McKenzie's uniform 1-D extension of a semi-infinite lithosphere is replaced with more realistic localised extension of the area corresponding to the reported width of the basin. We later show that the flexure and inelastic effects significantly change the geometry of the crust and Moho. It thus appears that McKenzie's coefficient $\beta$ is quite difficult to measure on the basis of observations of the Moho and crustal geometry (see also [30]). Following Royden and Keen [2] we can allow two coefficients of extension, $\beta$ and $\gamma$, for the crustal and mantle lithosphere, respectively (Fig. 3). In this paper, $\beta = \gamma$.

#### 2.4.2. Modelling of rifting stage

We decided to avoid modelling of the rifting stage because our general goal is to demonstrate the influence of such generally overlooked factors of rift evolution as erosion, lower-crustal flow and flexural weakening.

## 3. Results and discussion

### 3.1. Evolution of topography and crust

The topography produced by our fully coupled tectonic-erosion model predicts the form of flanks and basins observed in East Africa (e.g., Fig. 4a). The possibility that rifting did not yet stop in this region is also not crucially important because self-similar form-amplitude is only varied.

In many cases the initial paleo-geometry of the rift basin can be predicted from the data on the sedimentary sequences (e.g., [14]), though most of reconstructions are based on model assumptions. Here we do not try to reconstruct the true paleo-configuration of the rift, but instead we use various starting configurations of topography/Moho to determine the configuration which provides a best fit between with the present-day topography, geometry of the basement and Moho. We used $\beta$ between 1.25 and 2, which is believed to be reasonable for East African rifts [48]. We examine different values of the erosion coefficients (from 3,000–7,500 $m^2/y$ for zero-order erosion to 100,000 $m^2/y$ for first-order non-linear erosion, Fig. 4b) to obtain realistic volumes and rates of sedimentation and erosion.

Fig. 4a shows the evolution of the surface topography and Moho where the surface erosion and subsurface processes (rebound and flow) are coupled. It particularly shows that after some initial period of time, decay of the rift shoulders can be significantly slowed down and their geometry becomes stable. Dependent on the balance between the surface and subsurface processes, the subsidence may occur both at faster and lower rates than those predicted by McKenzie's model. The differences with the classical model constitute 10–20% to 50% in ultimate cases. Fig. 4a also shows that the velocity of subsidence is quite different in different parts of the basin.

In the model, coupling between the surface and subsurface processes can persist during substantially long periods of time ($> 30$ Ma), generally limited by space problems. In reality, the system eventually can get unbalanced much earlier, because the surface and subsurface processes are controlled by a number of independent factors such as climate (for erosion) and far field stresses (for the subsurface processes). This

unbalance can be followed by some oscillations in the subsidence rate.

Fig. 4b (top) illustrates that without feedback between surface and subsurface processes the elevated topography would be rapidly wiped out. If coupling is settled, the rift flanks persist for much longer time even for quite intensive erosion (Fig. 4b, middle and bottom).

### 3.2. Weakening effects and lower-crustal flow

As the basin is filled with sediments produced by erosion on the flanks, the lithosphere bends and mechanically weakens due to inelastic effects caused by flexural stress and thermal blanketing of the crust [7]. The blanketing may increase the temperature by 50–100°C at depths of about 15 km, which is equivalent to decrease of the yielding strength (quartz) there by a factor of 2. The erosion of the rift shoulders results in unloading of the lithosphere followed by a compensating isostatic uplift. The flexural stress propagates from the centre of the basin towards the shoulders (Fig. 5a) and causes their uplift, which leads to a compensating increase of the erosion rate. The load exerted on the plate by the uplifted rift shoulders weakens the lithosphere beneath them (Figs. 5 and 6, top), and this effect facilitates localization of the uplift of the shoulders in time. Flexural stresses created by irregular topography/sedimentary load can be 3–5 times higher (300–500 MPa) than the excess normal pressure associated with the weight of the topography/sediments itself ($< 100$ MPa). In the depth interval 15–25 km, the flexural stresses can exceed the total (lithostatic) pressure [17]. Fig. 5a demonstrates this effect of the irregularly distributed surface load on the stress field in the lithosphere. The figure also shows that the elastic cores are greatly reduced ($\sim 40\%$) and strain is localised in the area below the basin and rift shoulders. The effect of flexural weakening becomes even more important than the effects of thermal insulation, though the degree of flexural weakening is conditioned by temperature. Nevertheless, weakening results in additional subsidence which also changes the temperature regime of the lithosphere. Therefore, the stress-weakening effects and temperature-weakening effects are interdependent.

Subsidence of the basin creates pressure gradients in the lower crust directed towards the shoulders. The low-viscosity crustal material flows from underneath the basin towards the rift shoulders, causing additional uplift (Fig. 5b). This process somehow facilitates additional crustal thinning in the area of necking (Fig. 5a). However, without erosion-accelerated subsidence and uplift of the rift shoulders, the direction of the flow may become reversed: under the load of rift shoulders the lower-crustal material may start to flow backwards to the centre of the basin and result in its uplift or in retardation of subsidence. The shoulders then will collapse in time. Thus the erosion might be a leading factor that prevents collapse of the rift shoulders and regulates the rate of subsidence.

It should be noted that without areas of localized weakening beneath the basin and shoulders, the effect of the crustal flow could be less important. This is because in a plate with constant rigidity, the flexural stresses created by ascending flow beneath the rift shoulders would propagate on much longer distances. This may prevent subsidence of the basin, resulting in attenuation of the flow. The inelastic rheological effects thus must be very important in the evolution of the basin.

### 3.3. Influence of the erosion law

The isostatic uplift of the shoulders in response to the erosion is an important mechanism that maintains the relatively high rate of the material flux from the hillslopes. However, erosion of the divides results in their retreat from the centre of the basin. At the same time the sedimentary wedge migrates towards the centre of the basin (Figs. 4b and 5a, [49]). Such migration of the sedimentary load causes stress variations and characteristic stratigraphic onlap patterns that can be matched with the observations. The geometry of the rift shoulders and stratigraphic patterns are also highly dependent on the assumed erosion law. We used a zero-order short-range diffusion equation (2) for the short-range erosion and assumed flat deposition as a response to long-range fluvial transport surface processes. The transition from short-range to long-range processes was introduced for simplicity by the assumption that flat-de-

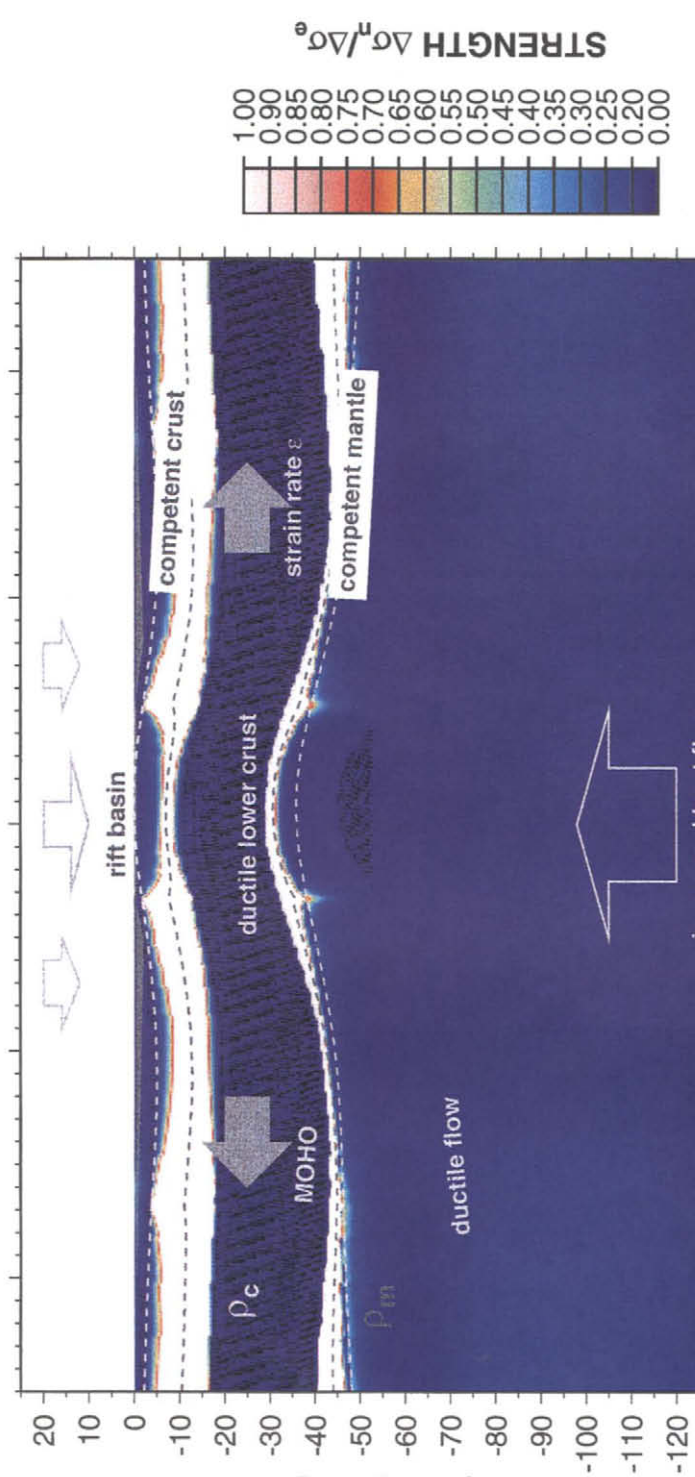


Fig. 5. a. Strength variations in lithosphere caused by inhomogeneous load (semi-analytical approximation). *White areas* correspond to the maximum strength. *Darker areas* indicate weakened inelastic material.

b. Flow lines in the lower crust at time $t = 10$ Ma (displacement field is not shown, see Fig. 5a). *Top*: Relatively rapid erosion and sedimentation ($K_s = 7500\ m^2/y$). The flow is directed outward from the centre of the basin towards the rift shoulders, facilitating their uplift and subsidence of the basin. The flow field is obtained by semi-analytical approach. *Bottom*: No erosion/sedimentation: the flow pattern is reversed, meaning gravity collapse of the rift. The flow field is obtained using numerical (finite element) solution (used for cross-checks with the semi-analytical solution).

position "switches on" at highs below 100 m from the outer side of the shoulders. We also tested first-order non-linear erosion to check the importance of the erosional law. The major effect is that it tends to keep the hillslopes more steep than in the linear erosion case (Fig. 4b). Thus it favours more localization of the rift shoulders than the conventional erosion law. The relief produced by the non-linear erosion is also more realistic than the relief produced by the linear erosion.

When the erosion is low, subsidence of the basins is retarded. The related pressure gradient might not be sufficient to counter-act the pressure gradients due to density contrasts between the crust and mantle beneath the rift shoulders. The net flux in the lower crust can be reversed in this case (Fig. 5c). It will

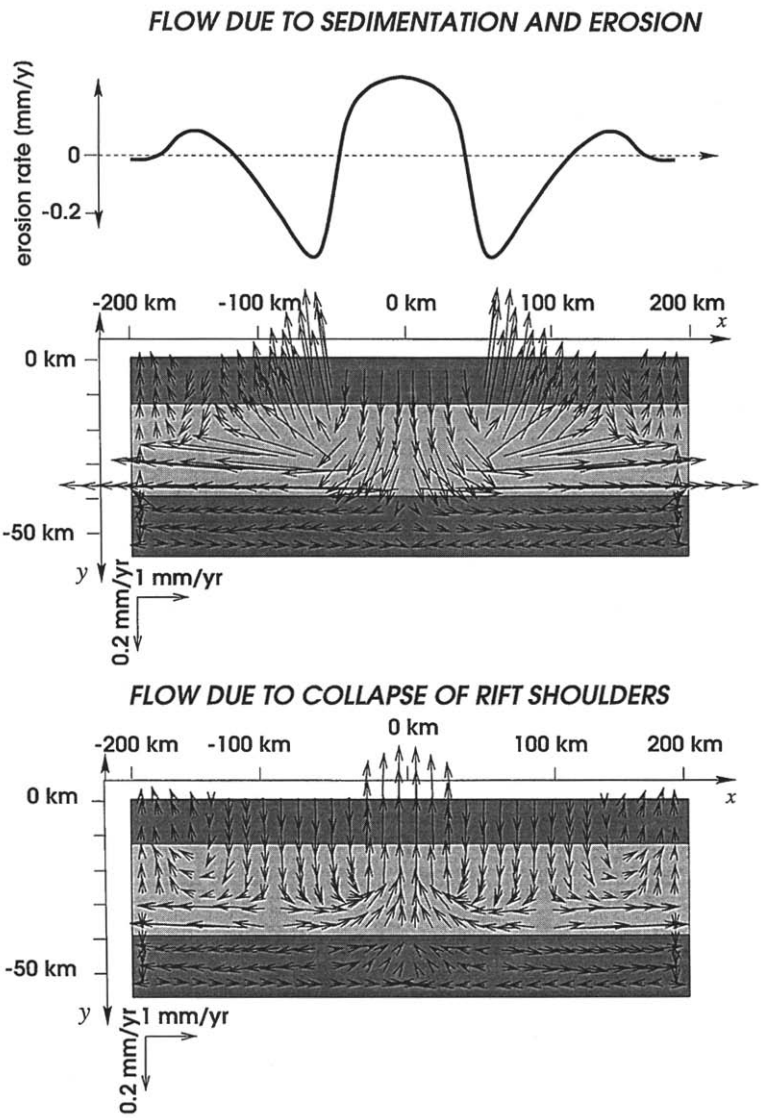


Fig. 5b (continued).

thus retard subsidence of the basin and accelerate collapse of the rift shoulders.

### 3.4. Temporal and spatial variations of the effective elastic thickness (EET) and basin geometry — Post-rift extension and compression

Fig. 6 shows comparison of the effective elastic thickness (EET, depth-integrated strength of the lithosphere) predicted by our model with EET predicted on the base of the classical McKenzie model of pure conductive cooling (assuming that competent crust and competent mantle are delimited by the isotherms 250–300°C and 700–750°C, respectively; e.g., [17]). As can be observed, for the specific but quite realistic case shown in Fig. 5a, the average EET does not significantly increase with time whilst the classical model [1] predicts a gradual increase of the lithospheric strength. According to our model, EET may even decrease in time for the cases of much larger basins like Pannonian or Dnieper–Donets shown in Fig. 2. Thus, one of the most conspicuous results is that the effects of cooling can be entirely compensated by the opposite effects of thermal insulation and weakening. The geometry of deflected basement produced by our model is also remarkably different from that which could be deduced using McKenzie's model — it more corresponds to the patterns produced by a model of local compensation beneath the most thick sediments. For less loaded areas the compensation is much more regional and cannot be explained by the assumption of local isostasy or low EET (this is in fact observed in the Albert rift [50]). Therefore, using a zero or constant EET for the basin would not accurately predict its subsidence history because all the back-

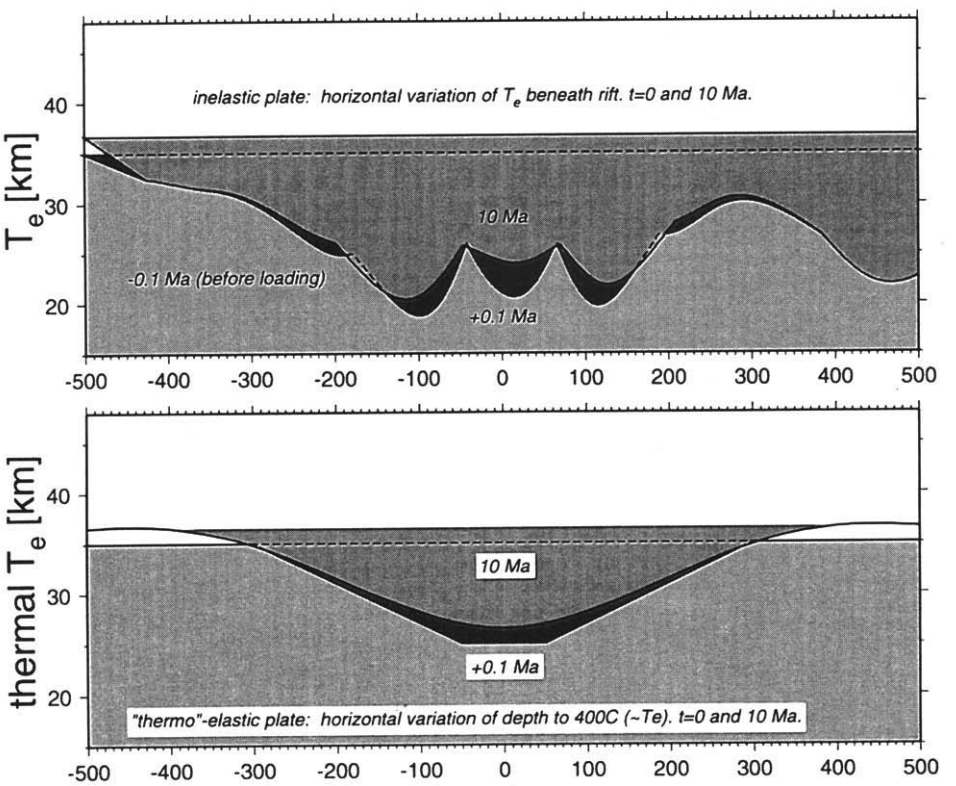


Fig. 6. Variation of EET. *Top*: Variation of EET due to surface loading produced by our model (case of Fig. 5a). *Bottom*: the reference McKenzie [1] model. Our model predicts smaller or no increase of EET in time, and localised reductions of EET beneath basin and shoulders. This helps localisation of the tectonic uplift/subsidence in time and prevents widening of the basin (gravity forces and erosional retreat of the drainage divides may actually widen the rift basin).

stripping techniques imply either constant, or zero EET, or thermally controlled EET growing in time (e.g., [3]).

The accumulation of the eroded matter requires as well an adequate increase of the basin volume in time. This can occur both in the vertical and horizontal directions, by an increase of the depth of the basin due to subsidence but also by progressive horizontal spreading and onlap of sedimentary deposits. A logical effect of the latter process is widening of the basin resulting in additional extension. This quasi-extension is facilitated by real post-rift extension due to diverging flow in the lower crust (Fig. 5b). As was noticed before, in the case of gravitational collapse, the flow in the lower crust might be reversed, thus facilitating post-rift compression (Fig. 5c).

In reality, the erosion cannot respond immediately to the changes in the surface uplift, particularly because it is also conditioned by a number of independent factors such as climate. As well, some time is needed for the lower crust to respond to changes in the surface load. This naturally may introduce some retardation in the feedback between the surface and subsurface processes. As it is well known from operational theory, delays in the feedback can result in oscillations in the system, especially in cases of rapid changes on input or in the feedback "loop". Therefore, one can predict a possibility of extensional and compressional oscillations, as well as of oscillations in the rate of subsidence caused by temporal unbalances between the forces of the gravity collapse, lower-crustal flow and erosion. Such oscillations in the rate of basin subsidence are indeed observed is several cases (e.g., Dnieper–Donets basin, J.-P. Le Nindre, pers. commun., 1996). Though they can be probably explained by eustatic changes, the "feedback" nature is also not excluded.

## 4. Conclusions

Although the main mechanism of crustal thinning — horizontal extension — retains its leading role in extensional basin formation, the additional strength decrease due to the vertical loading also appears to be important. In particular, this may change the amplitude (or rate) of subsidence by 10–20%. Plate weakening due to vertical loading should also facilitate extension. Evolution of the surface load in time due to sedimentation in the hinterland and erosion in higher flank areas continuously changes the strength of the underlying lithosphere. Because the flexure and inelastic effects significantly change the geometry of the crust and Moho, it appears that it is difficult to rely exclusively on estimates of the $\beta$-factor of extension made on the base of the observations of the crustal geometry or backstripping reconstructions.

We found that for young lithosphere, lateral and temporal $T_e$ variations due to sediment deposition may be more than 20%. This can lead to more than 10–15% difference in the geometry of the basement predicted by the traditional linear models. This suggests that the results of back-stripping reconstructions based on the assumption of a zero, or non-zero but constant, or only age/temperature dependent $T_e$, may require some reconsideration.

The evolution of a sedimentary basin and rift shoulders is to a large extent a result of coupling between surface processes (erosion and sedimentation) and the response of the lithosphere that includes both rebound, effects of localized weakening due to load and flow in the lower crust. Flow in the lower crust may facilitate both subsidence and crustal thinning, uplift of the rift shoulders and variation in the width of the basin (secondary extension). If erosion or subsidence has terminated for some reason, the lower-crustal flow will facilitate collapse of rift shoulders and thickening of the crust and uplift of the basin.

As demonstrated by our modelling, the effects of thermal insulation and of localized weakening of the lithosphere beneath the basin by flexural stress may retard or even entirely compensate the effects of conductive cooling predicted by conventional models.

It is generally believed that the rate with which the lithosphere accommodates changes in load is proportional to the characteristic relaxation time of the underlying asthenosphere. We show, however, that it is also controlled by lithospheric strain rates and rheology of the lithosphere itself. Kusznir and Karner [51] suggested that lithosphere older than 100 Ma will undergo no observable relaxation, but later studies (e.g., [22,25,52,42]), and this particular study,

demonstrate that the presence of low-viscosity lower crust with short relaxation time may introduce an important time-dependent contribution to the mechanical response of the lithosphere. This effect must be taken into account not only in the basin modelling, but also in the models of postglacial rebound of the lithosphere used to determine the effective viscosity of the asthenosphere.

One can predict some extensional and compressional oscillations, as well as oscillations in the rate of subsidence caused by temporal unbalances between the forces of the gravity collapse, lower-crustal flow and erosion.

## Acknowledgements

We gratefully thank C. Ebinger and J. Hopper for providing useful rigorous reviews. We are also indebted to G. Ranalli for numerous discussions on the rheological properties of quartz aggregates. Figs. 4–6 were prepared using graphics package GMT v. 3.0 by P. Wessel and W. Smith. This study was partially supported by IPGP (Paris) and ILP. NSG publication No. 97.09.09. ***UC***

## Appendix A

### *A.1. Coupled flexure / channel flow model of the lithosphere*

Bird [22] and Lobkovsky and Kerchman [24] give an analytic solution for evolution of the topography $\partial h/\partial t$ due to flow in the crustal channel for the case of local isostatic equilibrium. Kaufman and Royden [25] provide a solution for the case of an elastic mantle lithosphere. For the case with non-linear brittle–elasto-ductile crust and lithosphere no analytic solution can be found and we thus choose a semi-analytic approach.

The total uplift associated with the flow of the material in the ductile crust (initial thickness $\Delta h_0(x,0)$) can be defined as $\mathrm{d}u(x,t) = \mathrm{d}h(x,t) + \mathrm{d}e(x,t)$ (see Section 2.1 and Appendix A). The normal load (sum of the weight of the topography $p_+(x)$ and of the upper-crustal layer of thickness $h_{c1}$ and density $\rho_{c1}$), is applied to the upper wall of the lower-crustal layer (density $\rho_{c2}$) through the flexible strong upper-crustal layer. The vertical deflection $w$ of the strong upper mantle (Moho) is dependent on the undulation of the upper-to-lower crust interface $\tilde{h}$.

This lower-crustal layer of variable thickness $\Delta h_{c2} = \Delta h_0(x,0) + \tilde{h} + w$ is supported by the strength of the underlying mantle lithosphere (density $\rho_m$). Variation of the elevation of its upper boundary $\mathrm{d}\tilde{h} \approx \mathrm{d}u$ with respect to the undisturbed thickness $\Delta h_0(x,0)$ leads to variation of the normal load applied to the mantle lithosphere. Then, the lower boundary of the lower-crustal layer (i.e., Moho boundary) is $h_c(x,t) = \Delta h_{c2} + h_{c1}$. The value of $\tilde{h}$ is: $\tilde{h}(x,t) - \tilde{h}(x,t-\mathrm{d}t) = \mathrm{d}u - \mathrm{d}y_{13}$, where $\mathrm{d}y_{13} = y_{13}(x,t) - y_{13}(x,t-\mathrm{d}t)$ is the relative variation of the lower boundary of the elastic core of the upper crust due to local changes in the level of deviatoric stress. The flexure- and flow-driven deviatoric stresses can weaken material and thin, or "worn out" the bottom of the strong upper crust. The topographic elevation $h(x,t)$ can be defined as $h(x,t) = h(x,t-\mathrm{d}t) + \mathrm{d}\tilde{h} - \mathrm{d}e(t) - \mathrm{d}y_{13}$, where $dy_{13}$ would have a meaning of "subsurface erosion" of the crustal root due to inelastic deformation. The equations of motion for the incompressible fluid (lower crust) are [44]:

$$\sigma_{xx} = 2\mu\frac{\partial u}{\partial x} - P;\ \sigma_{xy} = \mu\left(\frac{\partial u}{\partial y} + \frac{\partial v}{\partial x}\right);$$

$$\sigma_{yy} = 2\mu\frac{\partial v}{\partial x} - P \qquad \text{(A-1)}$$

where $\mu = \sigma/2\dot{\varepsilon}$ is the effective viscosity; $P$ is pressure; and $u$ and $v$ are the horizontal and vertical components of the velocity, respectively.

This could be also written in the Navier–Stokes formalism [44]:

$$\rho_{c2}\cdot \mathrm{d}u/\mathrm{d}t = \rho_{c2}F_x - \partial P/\partial x + \partial/\partial y\left[2\mu\{(\partial u_{c2}/\partial x + \partial v_{c2}/\partial y)\}\right]$$

$$\rho_{c2}\cdot \mathrm{d}v/\mathrm{d}t = \rho_{c2}F_y - \partial P/\partial y + \partial/\partial x\left[2\mu\{(\partial u_{c2}/\partial x + \partial v_{c2}/\partial y)\}\right] \qquad \text{(A-2)}$$

where $F$ is a body force, in our case associated with shear on the slopes of the upper and lower channel

boundaries: $F_x \approx g\mathrm{d}\tilde{h}/\mathrm{d}x$, $F_y \approx g(1-\mathrm{d}\tilde{h}/\mathrm{d}x)$ at the upper channel interface and $F_x \approx g\mathrm{d}w/\mathrm{d}x$, $F_y \approx g(1-\mathrm{d}\tilde{h}/\mathrm{d}x)$ at the Moho (the sign $\approx$ means "approximately equal"). The horizontal pressure gradient $\mathrm{d}P/\mathrm{d}x$ is proportional to $\mathrm{d}(h+w)/\mathrm{d}x$; the vertical pressure gradient $\mathrm{d}P/\mathrm{d}y$ is $\sim \rho_{c2} g$. Within the narrow lower-crustal layer, the horizontal component of stress equilibrium equation $\mathrm{div}\,\sigma + \rho g = 0$, where $\sigma = \tau - PI$ is the deviatoric stress tensor, can be locally simplified to: $\partial\tau_{xy}/\partial y = \partial P/\partial x = -\partial\tau_{yy}/\partial x$ (e.g., [24,22]). A basic effective shear strain-rate can be evaluated as $\dot{\varepsilon}_{xy} = \sigma_{xy}/2\mu_{\mathrm{eff}}$. Then, assuming power law constitutive relations, the horizontal velocity $u_{c2} = u_x$ in the lower crust is:

$$u_{c2}(\tilde{y}) = \int_{h_{c1}}^{\tilde{y}} 2\dot{\varepsilon}_{xy}\partial\tilde{y} + C_1 = \int_{h_{c1}}^{\tilde{y}} 2^n A^* \exp[-H^*/RT(y)] \times |\tau_{xy}|^{n-1}\tau_{xy}\partial\tilde{y} + C_1 \quad \text{(A-3)}$$

Here $h_{c1}$ is the thickness of the competent upper crust, $\tilde{y} = y - h_{c1}$; $C_1$ is an arbitrary constant of integration, defined from boundary conditions. $\tau_{xy}$ is defined from integration of Eq. (A-3) by $y$.

The equation of motion for a thin layer in the approximation of lubrication theory will be:

$$\frac{\partial\tau_{xy}}{\partial y} - \frac{\partial P}{\partial x} = 0;$$

$$\frac{\partial P}{\partial y} \approx -\rho_{c2} g;\ \frac{\partial u_{c2}}{\partial y} = 2^n A^* (-H/RT)|\tau_{xy}|^{n-1};\ \frac{\partial v_{c2}}{\partial y} = -\frac{\partial u_{c2}}{\partial x} \quad \text{(A-4)}$$

where $\rho_c$ is averaged crustal density; $u_{c2}$ is the horizontal component of velocity of the differential movement in the lower crust; $v_{c2}$ is its vertical component; and $\partial u_{c2}(y)/\partial y$ is a component of shear strain rate in the lower crust. Strain rates of the lower-crustal rocks increase by factor of 2 for each $\sim 20$°C of temperature increase with depth (e.g., [22]). This results in that flow is concentrated at level of no shear [22,23,26] which is normally shifted to the Moho. Thus the effective thickness of the transporting channel is much less than $\Delta h_{c2}$. Because the viscosity of the lower crust is 2–4 orders of the magnitude lower than that of the surroundings (upper crust and mantle), its response to deformation of the surroundings can be considered as simultaneous.

Heat transfer equations (last equation of Eqs. 4), necessary to compute the rheological effects, are solved separately for the upper crust, lower crust and mantle lithosphere. The solutions for different layers are linked together through the conditions of temperature and heat flux continuity across the interfaces between the layers (see Table 1). The radiogenic heat term in Eqs. (4) is $H_r = \chi_{c1} k_{c1}^{-1} \rho_c H_s \exp(-yh_r^{-1})$ in the upper crust [39] (Table 1). $H_r$ equals $H_{c2} C_{c2}^{-1}$ in the lower crust and to zero in the mantle. The adiabatic temperature gradient in the asthenosphere, $\Omega$, is 0.3°C/km [39]. We first compute the initial geotherm for the thermal age $t_a$, then we compute the thermal perturbation due to extension according to [1]. The boundary and initial conditions are: $T(x,0,t_a) = 0$°C; $T(x,a_t,t) = T_m = 1330$°C ($a_t \approx 250$ km is the thermal thickness of the lithosphere); $T(x,y,0) = T_m$. $t_a$ is defined as the age of the last thermal event determined from geothermochronology and geomorphologic data.

## Appendix B

### *B.1. Flexure of a plate with inelastic (yield–strength) rheology*

For a plate infinite in $z$ direction, the bending moment $M = M_x$, longitudinal force component $T_x$ and vertical (shearing) force component $F_x$ per unit width are as follows [17]:

$$M_x = -\sum_{i=1}^{n}\int_{y_i^-}^{y_i^+(\phi)} \sigma_{xx}(x,y)\, y_i^*(\phi)\mathrm{d}y$$

$$T_x = -\sum_{i=1}^{n}\int_{y_i^-(\phi)}^{y_i^+(\phi)} \sigma_{xx}(x,y)\mathrm{d}y \quad \text{(B-1)}$$

$$F_x = -\sum_{i=1}^{n}\int_{y_i^-(\phi)}^{y_i^+(\phi)} \sigma_{xy}(x,y)\mathrm{d}y = \frac{\partial M_x}{\partial x}$$

where $\phi \equiv \{x,y,w,w',w''\}$ (see Table 1), $y_i^* = y - y_{ni}(\phi)$, $y_{ni}$ is the depth to the neutral plane of $i$th

elastic core of the multi-layered plate; $y_i^-(\phi) = y_i^-$, $y_i^+(\phi) = y_i^+$ are the depths to the lower and upper low-strength interfaces, respectively, thus $y_i^+ - y_i^- = \Delta h_i(\phi)$ is the thickness of the $i$th detached layer.

For a inelastic plate, we define a non-linear rigidity function $\tilde{D} = \tilde{D}(\phi)$ such as [59,17]:

$$\tilde{D}(\phi) \cdot \partial^2 w(x)/\partial x^2 \approx -\tilde{D}(\phi) R_{xy}^{-1} = -\tilde{M}_x(\phi) \tag{B-2}$$

Then we can define the effective elastic thickness $\tilde{T}_e = \tilde{T}_e(\phi)$ as:

$$\begin{aligned} \tilde{T}_e &= \left[\tilde{D}(\phi) L^{-1}\right]^{1/3} \\ &= \left[-\tilde{M}_x(\phi) R_{xy} L^{-1}\right]^{1/3} \\ &\approx \left[\tilde{M}_x(\phi) L^{-1} \left\{\partial^2 w(x)/\partial x^2\right\}^{-1}\right]^{1/3} \end{aligned} \tag{B-3}$$

where $L = E[12(1-\nu^2)]^{-1}$ and $R_{xy} \approx -(w'')^{-1}$ is the radius of plate curvature. $\tilde{D}$ and $\tilde{T}_e$ can be obtained from solution of the system (B-1) and plate equilibrium equation $(-\partial^2 M_x/\partial x^2 + \partial/\partial x (T_x \partial w/\partial x) + p_- = p_+)$ [17] with relations $\sigma_{xx}$ and strains $\varepsilon_{xx} = \varepsilon_{xx}(\phi)$ in Eqs. B-1 defined from the constitutive laws (see Section 2.2). $p-(w,x)$ is the buoyancy restoring force per unit area and $p_+(x)$ is the surface load.

## References


[1] D. McKenzie, Some remarks on the development of sedimentary basins, Earth Planet. Sci. Lett. 40 (1978) 25–32.

[2] L. Royden, C.E. Keen, Rifting process and thermal evolution of the continental margin of Eastern Canada determined from subsidence curves, Earth Planet. Sci. Lett. 51 (1980) 343–361.

[3] A.B. Watts, M. Torne, Crustal structure and the mechanical properties of extended continental lithosphere in the Valencia through (western Mediterranean), J. Geol. Soc. London 149 (1992) 813–827.

[4] M.H.P. Bott, Evolution of young continental margins, Tectonophysics 11 (1971) 319–327.

[5] N. White, D.P. McKenzie, Formation of the "Steer's Head" geometry of sedimentary basins by differential stretching of the crust and mantle, Geology 16 (1988) 250–253.

[6] J. Braun, C. Beaumont, A physical explanation of the relation between flank uplifts and the breakup unconformity at rifted continental margins, Geology 17 (1989) 760–765.

[7] R.A. Stephenson, S.M. Nakiboglu, M.A. Kelly, Effects of asthenosphere melting, regional thermoisostasy, and sediment loading on the thermomechanical subsidence of extensional sedimentary basins, R.A. Price (Ed.), Geophys. Monogr. 48 (1989) 17–27.

[8] P. England, S.W. Richardson, The influence of erosion upon the mineral facies of rocks from different metamorphic environments, J. Geol. Soc. London 134 (1977) 201–213.

[9] P. England, S.W. Richardson, Erosion and the age dependence of the continental heat flow, Geophys. J.R. Astron. Soc. 62 (1980) 421–437.

[10] S.A.P.L. Cloetingh, M.J.R. Wortel, N.J. Vlaar, Evolution of passive continental margins and initiation of subduction zones, Nature (London) 297 (1982) 139–142.

[11] S. Cloetingh, E.B. Burov, Thermomechanical structure of European lithosphere: constraints from rheological profiles and EET estimates, Geophys. J. Int. 124 (1996) 695–723.

[12] C. Beaumont, P. Fullsack, J. Hamilton, Erosional control of active compressional orogens, in: K.R. McClay (Ed.), Thrust Tectonics, Chapman and Hall, London, 1992, pp. 1–31.

[13] J. Chéry, F. Lucazeau, M. Daignieres, J.-P. Vilotte, Large uplift of rift flanks: A genetic link with lithospheric rigidity?, Earth Planet. Sci. Lett. 112 (1992) 195–211.

[14] P. van der Beek, P. Andriessen, S. Cloetingh, Morphotectonic evolution of rifted continental margins; inferences from a coupled tectonic-surface processes model and fission-track thermochronology, Tectonics 14 (1995) 406–421.

[15] G. Ranalli, Rheology of the Earth, 2nd ed., Chapman and Hall, London, 1995, 413 pp.

[16] G. Bassi, Relative importance of strain rate and rheology for the mode of continental extension, Geophys. J. Int. 122 (1995) 195–210.

[17] E.B. Burov, M. Diament, The effective elastic thickness ($T_e$) of continental lithosphere: What does it really mean?, J. Geophys. Res. 100 (1995) 3905–3927.

[18] C.J. Ebinger, T.D. Bechtel, D.W. Forsyth, C.O. Bowin, Effective elastic plate thickness beneath the East African and Afar Plateaux and dynamic compensation of the uplifts, J. Geophys. Res. 94 (1989) 2883–2901.

[19] M. Rohrman, P. van der Beek, P. Andriessen, S. Cloetingh, Meso-Cenozoic morphotectonic evolution of southern Norway: Neogene domal uplift inferred from apatite fission track thermochronology, Tectonics 14 (1995) 704–718.

[20] D.L. Kohlstedt, B. Evans, S.J. Mackwell, Strength of the lithosphere: Constraints imposed by laboratory experiments, J. Geophys. Res. 100 (1995) 17587–17602.

[21] E.V. Artyushkov, Stresses in the lithosphere caused by crustal thickness inhomogeneities, J. Geophys. Res. 78 (1973) 7675–7708.

[22] P. Bird, Lateral extrusion of lower crust from under high topography in the isostatic limit, J. Geophys. Res. 96 (1991) 10275–10286.

[23] W.R. Buck, Modes of continental lithospheric extension, J. Geophys. Res. 96 (1991) 20161–20178.

[24] L.I. Lobkovsky, V.I. Kerchman, A two-level concept of plate tectonics: application to geodynamics, Tectonophysics 199 (1992) 343–374.

[25] P.S. Kaufman, L.H. Royden, Lower crustal flow in an extensional setting: Constraints from the Halloran Hills region, eastern Mojave Desert, California, J. Geophys. Res. 99 (1994) 15723–15739.

[26] J.R. Hopper, W.R. Buck, The effect of lower crustal flow on continental extension and passive margin formation, J. Geophys. Res. 101 (1996) 20175–20194.

[27] M.A. Carson, M.J. Kirkby, Hillslope Form and Processes, Cambridge Univ. Press, Cambridge, 1972, 475 pp.

[28] H. Gossman, Slope modelling with changing boundary conditions — effects of climate and lithology, Z. Geomorphol. N.F., Suppl. Bd. 25 (1976) 72–88.

[29] S.H. Kirby, A.K. Kronenberg, Rheology of the lithosphere: Selected topics, Rev. Geophys. 25 (1987) 1219–1244.

[30] P.A. Ziegler, Geodynamic processes governing development of rifted basins, in: F. Roure, N. Ellouz, V.S. Shein, I. Skvortsov (Eds.), Geodynamic Evolution of Sedimentary Basins, Int. Symp., Moscow, 1994, pp. 19–67.

[31] K.H. Olsen, Continental Rifts: Evolution, Structure, Tectonics, Devel. Geotectonics, 25, Publ. 264 of ILP, Elsevier, Amsterdam, 1995.

[32] P.A. Ziegler, S. Cloetingh, J.-D. van Wees, Dynamics of intra-plate compressional deformation: the Alpine foreland and other examples, Tectonophysics 252 (1995) 7–59.

[33] A.R. Gilchrist, M.A. Summerfield, Differential denudation and flexural isostasy in formation of rifted-margin upwarps, Nature (London) 346 (1990) 739–742.

[34] H. Kooi, C. Beaumont, Escarpment evolution on high-elevation rifted margins: insights derived from a surface processes model that combines diffusion, advection and reaction, J. Geophys. Res. 99 (1994) 12191–12210.

[35] M.R. Leeder, Denudation, vertical crustal movements and sedimentary basin infill, Geol. Rundsch. 80 (2) (1991) 441–458.

[36] W.I. Newman, D.L. Turcotte, Cascade model for fluvial geomorphology, Geophys. J. Int. 100 (1990) 433–439.

[37] M.J. Kirkby, A two-dimensional model for slope and stream evolution, in: A.D. Abrahams (Ed.), Hillslope Processes, Allen and Unwin, Boston, MA, 1986, pp. 203–224.

[38] G. Willgoose, R.L. Bras, I. Rodrigues-Iturbe, A coupled channel network growth and hillslope evolution model 1, Theory Water Res. 27 (1991) 1671–1684.

[39] D.L. Turcotte, G. Schubert, Geodynamics — Applications of Continuum Physics to Geological Problems, Wiley, New York, NY, 1982, 450 pp.

[40] J. Déverchère, F. Houdry, M. Diament, N.V. Solonenko, A.V. Solonenko, Evidence for a seismogenic upper mantle and lower crust in the Baikal rift, Geophys. Res. Lett. 17 (6) (1991) 1099–1102.

[41] D. Doser, D.R. Yarwood, Deep crustal earthquakes associated with continental rifts, Tectonophysics 229 (1994) 123–131.

[42] J.-P. Avouac, E.B. Burov, Erosion as a driving mechanism of intracontinental mountain growth?, J. Geophys. Res. 101 (1996) 17747–17769.

[43] H.J. Melosh, Mechanical basis for low-angle normal faulting in the Basin and Range province, Nature (London) 343 (1990) 331–335.

[44] G.K. Batchelor, An Introduction to Fluid Dynamics, Cambridge Univ. Press, Cambridge, 1967, 615 pp.

[45] N.J. Kusznir, The distribution of stress with depth in the lithosphere: thermo-rheological and geodynamic constraints, Philos. Trans. R. Soc. London, Ser. A 337 (1991) 95–110.

[46] S. Ellis, P. Fullsack, C. Beaumont, Oblique convergence of the crust driven by basal forcing: implications for length-scales of deformation and strain partitioning in orogens, Geophys. J. Int. 120 (1995) 24–44.

[47] L. Royden, Coupling and decoupling of crust and mantle in convergent orogens: Implications for strain partitioning in the crust, J. Geophys. Res. 101 (1996) 17679–17705.

[48] C.J. Ebinger, G.D. Karner, G.D. Weissel, Mechanical strength of extended continental lithosphere: constraints from the western rift system, Africa, Tectonics 10 (1991) 1239–1256.

[49] R. van Balen, P.A. van der Beek, S.A.P.L. Cloetingh, The effect of rift shoulder erosion on stratal patterns at passive margins: Implications for sequence stratigraphy, Earth Planet. Sci. Lett. 134 (1995) 527–544.

[50] N.M. Upcott, R.K. Mukasa, C.J. Ebinger, G.D. Karner, Along-axis segmentation and isostasy in the Western rift, East Africa, J. Geophys. Res. 101 (1996) 3247–3268.

[51] N. Kusznir, G. Karner, Dependence of the flexural rigidity of the continental lithosphere on rheology and temperature, Nature (London) 316 (1985) 138–142.

[52] C.H. Jones, J.R. Unruh, L.J. Sonder, The role of gravitational potential energy in active deformation in the south-western United States, Nature (London) 381 (1996) 37–41.

[53] M.E. Artemjev, E.V. Artyushkov, Structure and isostasy of the Baikal rift and the mechanism of rifting, J. Geophys. Res. 76 (1971) 1197–1211.

[54] C. Petit, E.B. Burov, J. Déverchère, On the structure and the mechanical behaviour of the extending lithosphere in the Baikal Rift from gravity modeling, Earth Planet. Sci. Lett. (1997) in press.

[55] R. Stephenson, EUROPROBE Intraplate Tectonics and Basin Dynamics Dnieper–Donets and Polish Trough working groups, Continental rift development in Precambrian and Phanerozoic Europe: EUROPROBE and the Dnieper-Donets Rift and Polish Trough basins, Sediment. Geol. 86 (1993) 159–175.

[56] A. Adam, M. Bielik, The image of the narrow continental rifts in the crustal and mantle physics in the Pannonian basin, Geophys. J. Int. (1997) submitted.

[57] G. Spadini, A. Robinson, S. Cloetingh, Western versus Eastern Black Sea tectonic evolution: pre-rift lithospheric controls on basin formation, Tectonophysics 266 (1996) 139–154.

[58] U.S. ten Brink, Z. Ben-Avraham, R.E. Bell, M. Hassouneh,

D.F. Coleman, G. Andreasen, G. Tibor, B. Coakley, Structure of the Dead Sea pull-apart Basin from gravity analyses, J. Geophys. Res. 98 (1993) 21877–21894.

[59] E.B. Burov, M. Diament, Flexure of the continental lithosphere with multilayered rheology, Geophys. J. Int. 109 (1992) 449–468.

[60] W.F. Brace, D.L. Kohlstedt, Limits on lithospheric stress imposed by laboratory experiments, J. Geophys. Res. 85 (1980) 6248–6252.

[61] A.K. Kronenberg, J. Tullis, Flow strength of quartz aggregates: Grain size and pressure effects due to hydraulic weakening, J. Geophys. Res. 89 (1984) 4281–4297.

[62] N.L. Carter, M.C. Tsenn, Flow properties of continental lithosphere, Tectonophysics 36 (1987) 27–63.